Femtosecond laser fabricated polymeric grating for spectral tuning

Journal of Physics Communications

PAPER

Femtosecond laser fabricated polymeric grating for spectral tuning

Daiying Zhang[1], Liqiu Men[2] and Qiying Chen[1,2]

[1] Department of Physics and Physical Oceanography, Memorial University of Newfoundland, St. John's, Newfoundland A1B 3X7, Canada
[2] Faculty of Engineering and Applied Science, Memorial University of Newfoundland, St. John's, Newfoundland A1B 3X5, Canada

E-mail: qiyingc@mun.ca

Keywords: spectral tuning, filters, femtosecond laser microfabrication

OPEN ACCESS

RECEIVED
25 July 2018

REVISED
27 August 2018

ACCEPTED FOR PUBLICATION
7 September 2018

PUBLISHED
19 September 2018

Abstract

By taking advantages of the two-photon polymerization induced by femtosecond laser and the versatility of the femtosecond laser microfabrication, we demonstrate a femtosecond laser microfabricated polymeric grating for spectral tuning, in which gratings of different thicknesses achieve gradual tuning of a white incident light into output lights of different colors ranging from cyan to red, which is in good agreement with the simulation. Through the selection of different grating parameters, the technique developed in this study offers the possibility to tailor the performance of the grating to achieve specific grating efficiency or complete extinction at specific wavelengths, which is promising for measurements and applications in spectroscopy, sensing, integrated optical systems, and biomedicine.

1. Introduction

Spectral tuning, broadly to say, any operation to achieve the selection, filtering, or control of wavelengths in order to obtain specific spectral components of light, is essential in measurements with extensive uses in spectroscopy, microscopy, sensing, photochemistry, lasers, and optical communication. In many of these applications, optical filters are used, such as prisms, gratings, acouto-optical filters, and liquid crystal tunable filters [1–7]. However, most of these bulky filters are usually not suitable for use in an integrated system. Recently, some miniaturized microelectromechanical systems (MEMS)-based or optical fiber based tunable gratings have been reported [8–11]. Wavelength tuning in the visible spectral range, commonly known as color filtering, is particularly important for applications, such as a color filter consisting of an array of annular apertures in a gold film for transmission measurement [12], a multilayered structure incorporating a subwavelength metal-dielectric grating for better reflection resonance and color effects [13], excitation of surface plasmonic effects in nanostructured materials [14–16], and plasmonic color filters adopting free-standing resonant membrane waveguides [17]. Most of these reported components are either relatively large in volume for use in free-space optics, costly in the fabrication techniques, or are mostly incompatible with integrated systems, especially for the case of biomedical applications, for example, a lab-on-a-chip platform, where footprint and the compatibility with the fluidic environment are crucial [18]. Yu *et al* showed an optical diffraction grating using multiphase droplets on a microfluidic chip, which produces different colors as a color filter [19]. Cuennet *et al* reported the integration of color filter with microfluidics by soft lithography for on-chip absorption spectroscopy, in which the tunable filter was based on the micro-flow of liquid crystals for its wavelength-dependent birefringence by modifying the flow velocity field in the microchannel [20]. These reported microfluidic filters were fabricated by standard soft-lithography relying on the movement of multiphase droplets or micro-flow of liquid crystals, in which the controllability and repeatability of the device performance could be significant concerns.

In this letter, we report a technique of femtosecond laser microfabricated polymeric grating and demonstrate its application in spectral tuning. In this study, gratings with an epoxy-based negative photoresist (SU-8) are fabricated by direct writing with a Ti:sapphire femtosecond laser at a wavelength of 800 nm, a pulse width of 67 fs, and a repetition rate of 80 MHz (Libra system, Coherent Inc.). Conventional techniques to

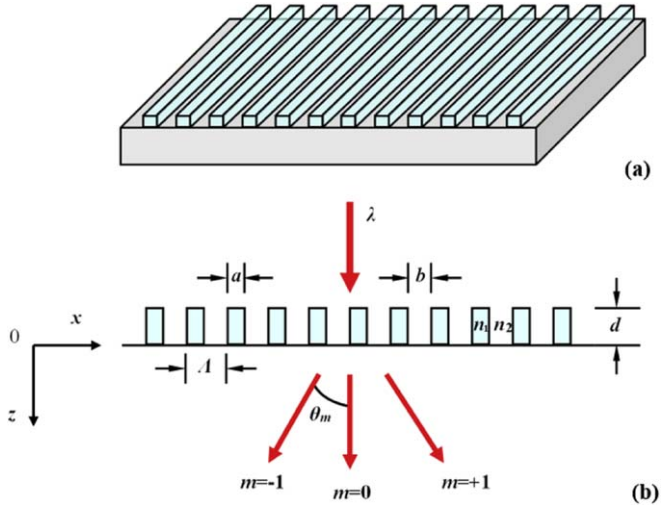

Figure 1. Schematic illustration of a guided-mode resonance grating: (a) the 3D view, and (b) the side view.

fabricate diffraction gratings include photo-masking [21], electron beam lithography [22], etching techniques [23], and holographic interference [24, 25]. Holographic lithography/recording was developed to create periodic 3D microstructures, in which periodic interference patterns such as an aspheric microlens structure [26], microscopic tubular structure [27], and fast bits [28], are printed into the photoresist by multi-laser beam irradiation. This technique for the fabrication of 3D microstructures possesses the merit of fast fabrication but requires higher laser power and is limited to patterns of interference. Recently, maskless femtosecond laser direct writing and femtosecond laser-assisted etching have been reported to achieve dynamically tunable protein microlens and tunable microlens, respectively [29, 30]. Despite the use of relatively slow line-by-line approach, the femtosecond laser microfabrication technique adopted in this study exhibits its salient advantages of flexibility and versatility, in which it is easy to write gratings with different specifications (periodicity Λ, thickness d, and width a) by simply adjusting the laser parameters (i.e., laser power, scan speed, and focusing condition), and thus offers the significant merits in the adjustability of the grating performance for measurements.

2. Principle

For the case of a diffraction grating, as shown in figure 1, the grating equation is:

$$\Lambda \sin \theta_m = m\lambda (\text{normal incidence}) \tag{1}$$

where θ_m is the angle between the mth order and the zeroth order diffracted rays, depending on the wavelength and the periodicity. When a white light passes through the grating, components of light with a single wavelength are separated into different directions, thus producing a dispersion spectrum. The intensity of the zeroth order of diffraction ($m = 0$) can be derived to relate with the thickness of the grating and the refractive indices (RIs) of the periodic regions based on the discussion in [31]:

$$\begin{aligned} I_0 &= 1 - 2\frac{a}{\Lambda}\left(1 - \frac{a}{\Lambda}\right) + 2\frac{a}{\Lambda}\left(1 - \frac{a}{\Lambda}\right)\cos\delta\varphi \\ &= 1 - 2\frac{a}{\Lambda}\left(1 - \frac{a}{\Lambda}\right) + 2\frac{a}{\Lambda}\left(1 - \frac{a}{\Lambda}\right)\cos\left[\frac{2\pi}{\lambda}d(n_1 - n_2)\right] \end{aligned} \tag{2}$$

where Λ is the grating pitch, d is the thickness of the grating, $\delta\varphi = \varphi_1 - \varphi_2$ is the phase difference, φ_1 and φ_2 are the phases of light that passes through the higher RI region n_1 and lower RI region n_2, and a and b are the widths of the two regions, respectively. Equation (2) indicates that the intensity of the zeroth order of diffraction depends on all grating parameters (Λ, a, d, n_1, n_2), as well as the wavelength of the incident light (λ), which suggests that, by either varying the thickness of the grating or adjusting the RI of the fluid flowing in the microchannels, the zeroth order of diffraction with different spectral features (color and intensity) can be observed by a charge coupled device (CCD) camera when a white light passes through the grating.

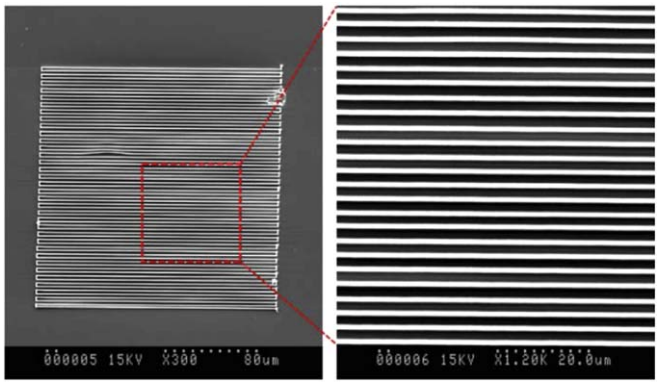

Figure 2. SEM images of a femtosecond laser microfabricated grating with a periodicity of 3 μm. The size of the grating is 200 μm $\times$ 200 μm.

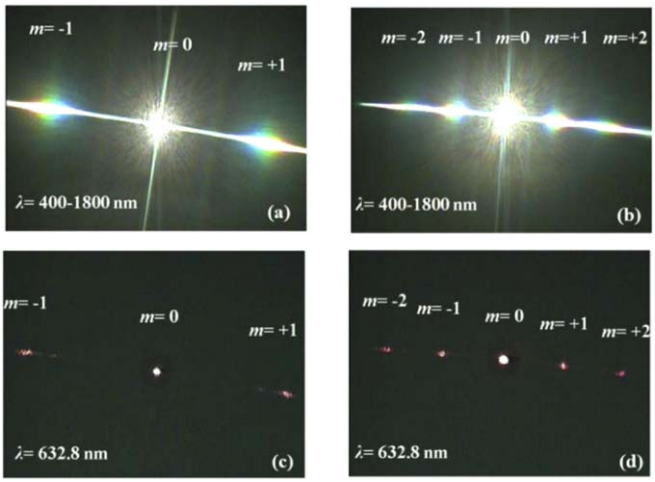

Figure 3. Diffraction patterns observed with a Panasonic CCD camera from a femtosecond laser microfabricated grating: (a) and (c), $\Lambda = 2$ μm; (b) and (d) $\Lambda = 3$ μm.

3. Results and discussion

Figure 2 shows the SEM images of a grating with a periodicity of 3 μm over a grating size of 200 μm $\times$ 200 μm, fabricated by a femtosecond laser power of 0.625 nJ/pulse and a scan speed of 20 μm/s when the laser beam is focused by a 50 $\times$ objective lens with a numerical aperture (NA) of 0.8. The width of the grating is 0.989 μm. These periodic channels exhibit high uniformity and excellent quality. The resolution of the femtosecond laser fabrication is mainly restricted by diffraction limit, in which the line width is inversely proportional to the value of the NA, i.e., a smaller feature can be crafted with an objective lens of a higher NA value. The selection of an objective lens with a suitable NA value is determined by the size of the microstructures to be created as well as other experimental considerations. The femtosecond laser focused by an objective lens of a higher NA fabricates a narrower and thinner line. As a result, multiple scans will be required in order to achieve a line on a photoresist film of larger thickness such as 2 μm or thicker, which will reduce the efficiency and effectiveness of the femtosecond laser microfabrication.

Figure 3 gives the diffraction patterns captured by the Panasonic CCD camera for the gratings with periodicities of 2 and 3 μm, respectively. Similar diffraction patterns have also been detected at the same site with the Hamamatsu camera head. It is obvious from the figure that $m = 0, \pm 1$ orders are shown on the screen for the grating with a periodicity of 2 μm and $m = 0, \pm 1, \pm 2$ orders observed for the grating with a periodicity of 3 μm. The light with a shorter wavelength is closer to the center of the zeroth order than the light of a longer wavelength for the same diffraction order which indicates that the shorter wavelength light has a smaller angle of diffraction. The diffracted light is closer to the center in a long-period grating than in a short-period grating at the same diffraction order manifesting a smaller angle of diffraction for a long-period grating. In addition, it can

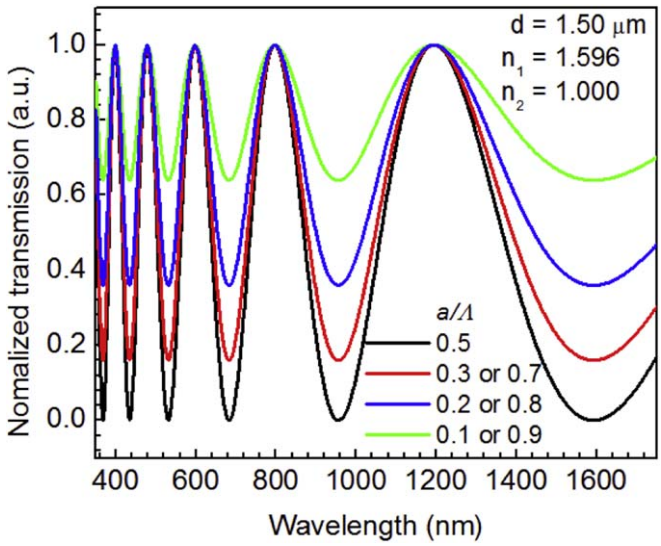

Figure 4. Simulation on the transmission spectra of the zeroth order in different duty cycles according to equation (2). The SU-8 grating is surrounded by air and the thickness of the SU-8 grating d is 1.50 μm.

also be found in figure 3(b) that the light with a longer wavelength in the first order partly overlaps with the light of a shorter wavelength in the second order of diffraction.

As the equation (2) reveals that the intensity of the zeroth order diffraction depends on the duty cycle a/Λ and a cosine function of $1/\lambda$, the simulated curves of I_0 in the wavelength range of 350–1750 nm at different ratios of a/Λ is given in figure 4, in which the thickness d is 1.50 μm, n_1 is 1.596 (the RI of SU-8 at 633 nm) [32], and n_2 is 1.000 (air), respectively. Multiple periods are observed in the spectral curves while the extinction ratio reaches its maximum at $a/\Lambda = 0.5$ and then diminishes with either an increase or decrease of a/Λ. It is obvious that the wavelengths of the peaks and valleys are independent of the grating's duty cycle a/Λ. Therefore, gratings with a periodicity of 2 μm at a duty cycle a/Λ of 0.5 and another periodicity of 5 μm at a duty cycle a/Λ of 0.2 are employed in this study to investigate the characteristics of the spectrum of the zeroth order diffraction.

If the phase difference satisfies

$$\delta\phi = \frac{2\pi}{\lambda} d(n_1 - n_2) = (2q + 1)\pi \tag{3}$$

where q is some integer, then the following relation can be derived:

$$\lambda = \frac{2(n_1 - n_2)}{2q + 1} d \qquad (I_0 = \text{minimum}) \tag{4}$$

Here, q is the order of the resonance mode. This equation tells that, once the phase difference equals an odd integer number of π, this specific monochromatic light is completely filtered out by a grating with a duty cycle (a/Λ) of 0.5. Therefore, equation (4) is the foundation to design grating color filters. In our experiments, the spectrum and intensity of the zeroth order diffracted light are measured by an optical spectrum analyzer (Ando AQ-6315, Japan). Normalized transmission (grating efficiency) is obtained by calculating the ratio of the intensity of the zeroth order diffracted light and that of the light source.

Figure 5 gives the transmission spectra of femtosecond laser microfabricated gratings with different grating thicknesses of 1.57, 1.76, 1.84, and 2.15 μm, which are measured by a 3D optical surface profiler (Nexview, Zygo Corp.). The thickness of the grating can be adjusted by either changing the focusing of the femtosecond laser or varying the thickness of the photoresist film through changing the rotation speed of the spin-coating while we have adopted the second approach in this study. The values of the parameter Λ in figures 5(a)–(c) are 2 μm, and 5 μm in figure 5(d). The results from the simulation with equation (2) by MATLAB software are also shown in the figures with the parameters a/Λ, n_1, and n_2 of 0.5, 1.596, and 1.000, respectively. The morphology of the gratings captured by a Leica DMR optical microscope (Germany) and the spots on the samples for spectroscopic measurement are also marked in the figures. The figure shows the measured normalized spectra of the zeroth order diffracted light from different samples along with the simulation results for comparison. Due to the fact that the RI changes slightly with varying wavelengths, there is a small discrepancy between the experimental data and the simulation results. For the S1 sample with a grating thickness of 1.57 μm, the transmission spectrum shows the highest intensity at 491.8 nm which corresponds to a cyan color for human eyes. For the samples S2, S3, and S4 with grating thicknesses of 1.76, 1.84, and 2.15 μm, the highest intensity is shown at a wavelength of

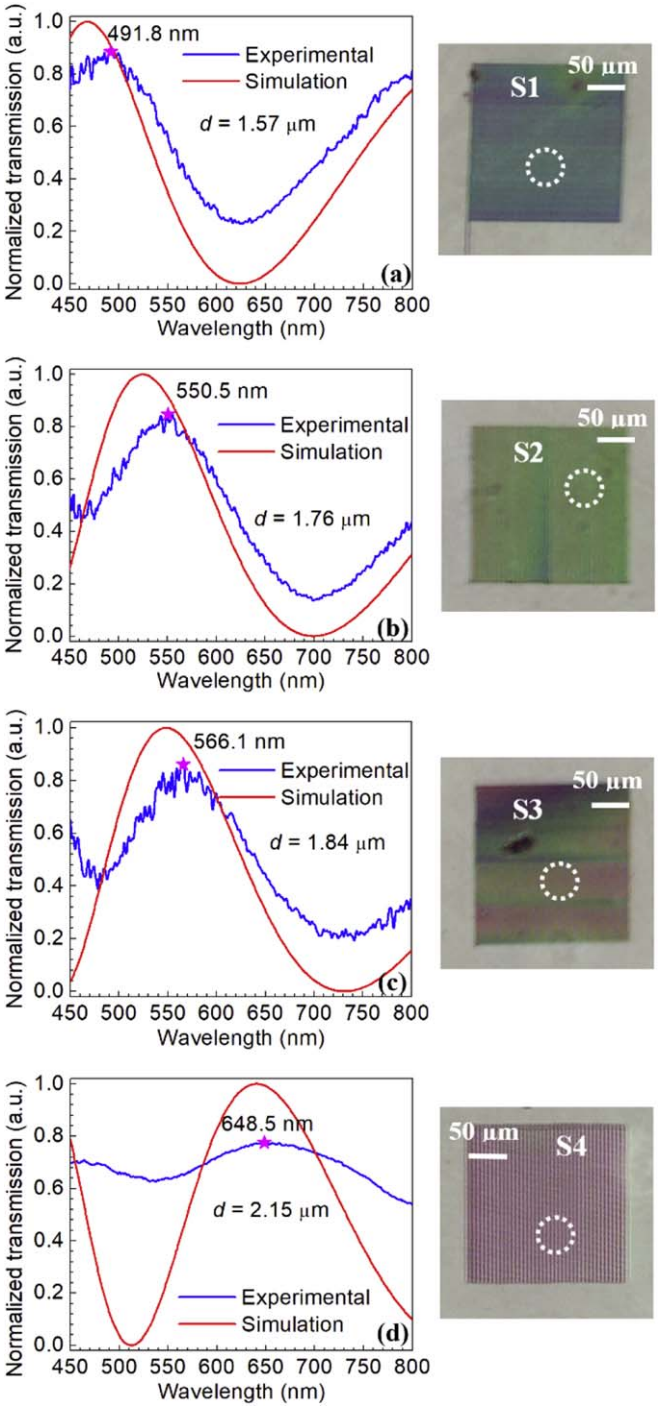

Figure 5. Transmission spectra of femtosecond laser microfabricated gratings with different grating thicknesses: (a) 1.57 μm; (b) 1.76 μm; (c) 1.84 μm; and (d) 2.15 μm. The values of parameter Λ and a/Λ in (a), (b), and (c) are 2 μm and 0.5, and 5 μm and 0.2 in (d), respectively. The simulation results with equation (2) by MATLAB software are also shown in the figures with the parameters a/Λ, n_1, and n_2 of 0.5, 1.596, and 1.000, respectively. The morphology of the gratings and the spots on samples for spectroscopic measurement are shown as well.

550.5, 566.1, and 648.5 nm, respectively, which corresponds to a color of green, yellow, and red for human eyes accordingly. The lights after the gratings of different thicknesses exhibit different colors under the microscope, which matches the fact that the chromaticity diagram depends on spectral features. It is noted that the experimentally observed transmission spectrum in figure 5(d) shows a smaller extinction ratio than the simulation result due to its smaller duty cycle. The values of the duty cycle are 0.2 and 0.5 for the experiment and the simulation, respectively.

Figure 6(a) shows a CIE 1931 color space chromaticity diagram [33]. The numbers along the outer curved boundary correspond to the wavelengths of the monochromatic light. The coordinates are calculated from the ratios of the *XYZ* tristimulus values [34, 35]. The chromaticity diagram describes the colors observed by human

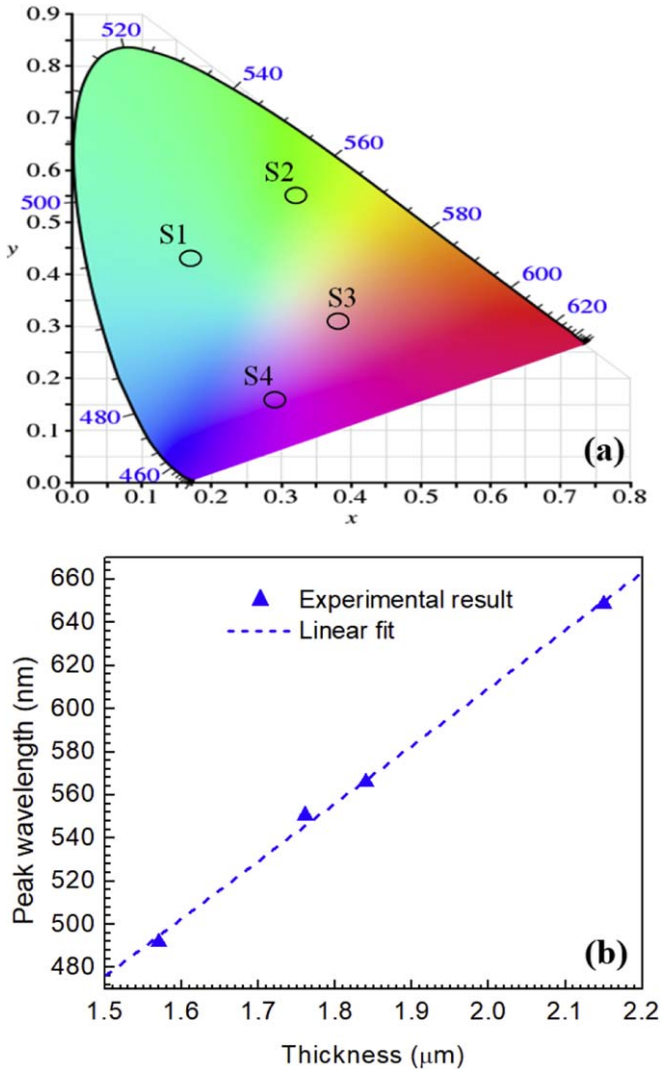

Figure 6. (a) The CIE 1931 color space chromaticity diagram. S1–S4 labelled in the figure correspond to the colors shown in figure 5(b) dependence of the peak wavelength on grating thickness for samples with their transmission spectra shown in figure 5.

eyes when monochromatic lights mix together with different intensities. S1–S4 labelled in figure 6(a) correspond to the colors shown in figure 5. The peak wavelength λ_{peak} with the same resonance mode are marked with star signs in figure 5. The experimental data in figure 6(b) show a linear relationship between the peak wavelength λ_{peak} and thickness d, in agreement with the prediction from equation (2) that the peak shifts to a longer wavelength as the thickness increases.

4. Conclusions

In summary, femtosecond laser microfabricated polymeric grating has been realized in this study and its application in spectral tuning has been demonstrated. Color tuning from the SU-8 gratings of different thicknesses is experimentally observed, which is in good agreement with the simulation. Compared with other reported grating-based color filters, the technique developed in this study is much powerful and versatile, which enables fabrication of high-quality grating with superior performance as a tunable color filter. It is worthy to mention that it is also possible to achieve spectral tuning over other spectral ranges in addition to the visible spectral range demonstrated here. The possibility to vary the values of the specifications of the gratings enables the feasibility to design and fabricate a variety of spectral tuning components for a wide range of applications. Furthermore, the grating and the femtosecond laser microfabrication technique developed in this study provide a platform technology to use the grating as a modular unit to enable the integration of multitude functionalities for a range of novel applications in measurement science and technology in the future.

Acknowledgments

This work has been supported by the Natural Sciences and Engineering Research Council of Canada (NSERC), Canada Research Chairs Program, Canada Foundation for Innovation, the Province of Newfoundland and Labrador, and the Memorial University of Newfoundland.

ORCID iDs

Qiying Chen https://orcid.org/0000-0002-2804-7121

References

[1] Born M and Wolf E 1999 *Principles of Optics: Electromagnetic Theory of Propagation, Interference and Diffraction of Light* 7th (Cambridge: Cambridge University Press)
[2] Mao X and Zeng L 2018 Design and fabrication of crossed gratings with multiple zero-reference marks for planar encoders *Meas. Sci. Technol.* **29** 025204
[3] Lu Z, Wei P, Wang C, Jing J, Tan J and Zhao X 2016 Two-degree-of-freedom displacement measurement system based on double diffraction gratings *Meas. Sci. Technol.* **27** 074012
[4] Zheng D, Yin S, Luo Z, Zhang J and Zhou T 2016 Measurement accuracy of articulated arm CMMs with circular grating eccentricity errors *Meas. Sci. Technol.* **27** 115011
[5] Lu P and Chen Q 2009 Optical low-coherence reflectometry for deflection measurement with a fiber Bragg grating cantilever sensor *Meas. Sci. Technol.* **20** 075303
[6] Kozlova O, Sadouni A, Truong D, Briaudeau S and Himbert M 2016 Tunable transportable spectroradiometer based on an acousto-optical tunable filter: development and optical performance *Rev. Sci. Instru.* **87** 125101
[7] Abuleil M and Abdulhalim I 2016 Narrowband multispectral liquid crystal tunable filter *Opt. Lett.* **41** 1957–60
[8] Huang N T, Truxal S C, Tung Y C, Hsiao A, Takayama S and Kurabayashi K 2009 High-speed tuning of visible laser wavelength using a nanoprinted grating optical tunable filter *Appl. Phys. Lett.* **95** 211106
[9] Lu P, Men L and Chen Q 2009 Wavelength control with gating imprinted fiber Sagnac loop mirror by polarization and strain tuning *J. Appl. Phys.* **106** 013111
[10] Men L, Lu P and Chen Q 2009 Spectral filtering using fibre Bragg grating embedded Sagnac loop mirror *Electron. Lett.* **45** 402–3
[11] Smietana M, Koba M, Mikulic P and Bock W J 2014 Tuning properties of long-period gratings by plasma post-processing of their diamon-like carbon nano-overlays *Meas. Sci. Technol.* **25** 114001
[12] Si G, Zhao Y, Liu H, Teo S and Zhang M 2011 Annular aperture array based color filter *Appl. Phys Lett.* **99** 033105
[13] Chen Y and Liu W 2012 Design and analysis of multilayered structures with metal-dielectric gratings for reflection resonance and color generation *Opt. Lett.* **37** 4–6
[14] Hynn J, Kang T, Baek H, Kim D and Yi G 2015 Nanoscale single-element color filters *ACS Nano Lett.* **15** 5938–43
[15] Li Z, Clark A W and Cooper J M 2016 Dual color plasmonic pixels created a polarization controlled nano color palette *ACS Nano* **10** 492–8
[16] Sun L B, Hu X L, Zeng B, Wang L S, Yang S M, Tai R Z, Fecht H J, Zhang D X and Jiang J Z 2015 Effect of relative nanohole position on color purity of ultrathin plasmonic subtractive colour filters *Nanotechnology* **26** 305204
[17] Wang J, Fan Q, Zhang S, Zhang Z, Zhang H, Liang H, Cao X and Xu T 2017 Ultra-thin plasmonic color filters incorporating free-standing resonant membrane waveguides with high transmission efficiency *Appl. Phys. Lett.* **110** 031110
[18] Zhang D, Men L and Chen Q 2011 Microfabrication and applications of opto-microfluidic sensors *Sensors* **11** 5360–82
[19] Yu J Q, Yang Y, Liu A Q, Chin L K and Zhang X M 2010 Microfluidic droplet grating for reconfigurable optical diffraction *Opt. Lett.* **35** 1890–2
[20] Cuennet J G, Vasdekis A E and Psaltis D 2013 Optofluidic-tunable color filters and spectroscopy based on liquid-crystal microflow *Lab Chip* **13** 2721–6
[21] Weichelt T, Bourgin Y and Zeitner U D 2017 *Mask aligner lithography using laser illumination for versatile pattern generation Opt Exp* **25** 20983–92
[22] Sudheer, Porwal S, Bhartiya S, Rao B T, Tiwari P, Srivastava H, Sharma T K, Rai V N, Srivastava A K and Naik P A 2016 Diffraction efficiency of plasmonic gratings fabricated by electron beam lithography using a silver halide film *J. Appl. Phys.* **120** 043101
[23] Wang S, Zhou C, Zhang Y and Ru H 2006 Deep-etched high-density fused-silica transmission gratings with high efficiency at a wavelength of 1550 nm *Appl. Opt.* **45** 2567–71
[24] Yu W and Yuan X C 2003 Variable surface profile gratings in sol-gel glass fabricated by holographic interference *Opt. Exp.* **11** 1925–30
[25] Zhang C, Hu Y, Li J, Lao Z, Ni J, Chu J, Huang W and Wu D 2014 An improved multi-exposure approach for high quality holographic femtosecond laser patterning *Appl. Phys. Lett.* **105** 221104
[26] Hu Y, Chen Y, Ma J, Li J, Huang W and Chu J 2013 High-efficiency fabrication of aspheric microlens arrays by holographic femtosecond laser-induced photopolymerization *Appl. Phys. Lett.* **103** 141112
[27] Zhang C, Hu Y, Li J, Li G, Chu J and Huang W 2014 A rapid two-photon fabrication of tube array using an annular Fresnel lens *Opt. Express* **22** 3983–90
[28] Hu Y, Ma J, Chen Y, Li J, Huang W and Chu J 2014 Fast bits recording in photoisomeric polymers by phase-modulated femtosecond laser *IEEE Photon. Technol. Lett.* **26** 1154–6
[29] Sun Y, Dong W, Yang R, Meng X, Zhang L, Chen Q and Sun H 2012 Dynmically tunable protein microlenses *Angew. Chem. Int. Ed.* **51** 1558–62
[30] Hu Y *et al* 2018 All-glass 3D optofluidic microchip with built-in tunable microlens fabricated by femtosecond laser-assisted etching *Adv. Opt. Mater.* **6** 1701299
[31] Grzybowski B A, Qin D and Whitesides G M 1999 Beam redirection and frequency filtering with transparent elastomeric diffractive elements *Appl. Opt.* **38** 2997–3002

[32] Sum T C, Bettiol A A, van Kan J A, Watt F, Pun E Y B and Tung K K 2003 Proton beam writing of low-loss polymer optical waveguides *Appl. Phys. Lett.* **83** 1707–9
[33] Smith T and Guild J 1931 The C.I.E. colorimetric standards and their use *Trans. Opt. Soc.* **33** 73–134
[34] Kosztyán Z T, Eppeldauer G P and Schanda J D 2010 Matrix-based color measurement corrections of tristimulus colorimeters *Appl. Opt.* **49** 2288–301
[35] Charrière R, Hébert M, Trémeau A and Destouches N 2016 Color calibration of an RGB camera mounted in front of a microscope with strong color distortion *Appl. Opt.* **52** 5262–71